Commun. Theor. Phys. **77** (2025) 055505 (14pp) https://doi.org/10.1088/1572-9494/ada37a
CSTR: 32041.14.CTP.ada37a

Co-existence of compressive and rarefactive dust acoustic solitary structures in Saturn's rings with non-Maxwellian ions and electrons

S A M Zaidi, M N S Qureshi* and Saba Khalid

Department of Physics, GC University Lahore, 54000, Pakistan

E-mail: noumansarwar@gcu.edu.pk

Received 18 October 2024, revised 27 December 2024
Accepted for publication 27 December 2024
Published 6 March 2025

Abstract

In the present study, we investigated the existence of arbitrary amplitude dust acoustic solitons by considering the Cairns distributed ions, negatively charged streaming dust grains along with (r, q) distributed electrons in an un-magnetized dusty plasma. We used the pseudopotential technique to obtain the solitary wave solution. It is seen that the coexistence of rarefactive and compressive solitons is possible when ions and electrons are nonthermally distributed. We found that the soliton characteristics are strongly dependent on the choice of velocity distribution function through the nonthermal spectral indices r, q, α as well as on the ion and dust temperatures. For (r, q) distributed electrons, we found that the soliton amplitude increases (decreases) with smaller (higher) values of negative (positive) r. For Cairns distributed ions, we found a transition from negative to positive polarity solitary structures with the coexistence in between as the nonthermal parameter α increases. Our results gave a better explanation for the formation of dust acoustic solitary structures and their dependence on high and low energy particles in nonthermal distribution profiles in space environments.

Keywords: dusty plasmas, generalized (r, q) distribution, non-Maxwellian distribution, dust acoustic waves, compressive and rarefactive solitons

(Some figures may appear in colour only in the online journal)

1. Introduction

In recent years, a significant increase in research on plasmas containing negatively charged dust particles has been seen; consequently, astrophysical environments and space are the most common places where these plasmas exist. A new wave mode, known as Dust Acoustic Wave (DAW), with an ultralow frequency domain, was theoretically predicted by Rao *et al* [1]. Numerous laboratory experiments [2, 3] have confirmed not only the existence of such waves but also showed that linear as well as nonlinear characteristics of plasma waves are strongly influenced by velocity distributions [4]. Several observations have pointed out that fast moving electrons and ions in space environments follow nonthermal distributions.

Experiments have shown that when a dust particle takes up ions or electrons from the plasma, it acquires a charge. Usually, dust particles get a negative charge; since electrons rapidly move towards them due to their smaller mass. Many authors have reported that DAWs exist in such complex plasmas where dust grains get a negative charge [1, 5–10]. The ultralow frequency DAW propagates due to the compression and rarefaction of dust particles, however, the thermal pressures of electrons and ions provide the restoring force.

DAWs with small but finite amplitude and cold dust were studied in un-magnetized dusty plasma [1], where electrons and ions were assumed to follow the Maxwellian distribution. Later, Mamun *et al* [5] studied DAWs with large amplitude in un-magnetized dust-ion plasma using the pseudopotential technique and reported that nonthermal distributed ions

* Author to whom any correspondence should be addressed.

considerably alter the solitary structures. Asgari *et al* [6] investigated the dust-acoustic solitary waves in dusty plasma with nonthermal ions and showed that for a given soliton speed, non-thermal ions broaden the dust-acoustic solitary wave and decrease its amplitude by increasing wave phase velocity. It is important to take non-thermal ion effects into account while studying dust-acoustic waves in space environments, as these findings imply important consequences. Mendoza-Briceno *et al* [7] investigated the dust acoustic waves with large amplitude in un-magnetized, hot, dust-ion plasma with Cairns distributed ions and reported the existence of both compressive and rarefactive waves. Further, they considered a relative streaming between the plasma and the charged particles in astrophysical environments. Gill and Kaur [8] employed the Sagdeev pseudopotential method, taking into account nonthermal ion distributions and finite dust temperature. They investigated nonlinear dust-acoustic waves in un-magnetized dusty plasma in accordance to the concentration of nonthermal ions, dust temperature, and Mach number. They found the co-existence of compressive and refractive solitons. The results demonstrate that while certain nonthermal ion concentrations eliminate refractive solitons, raising dust temperature reduces the range of soliton co-existence. The restoration of refractive solitons upon decreasing dust temperature at these concentrations emphasizes the interaction between dust temperature and ion dynamics in soliton behavior. Mahmood *et al* [9] reported that solitary structures were considerably modified in a dust–ion–electron dusty plasma due to the streaming velocity of dust. Misra and Wang [10] studied the dust acoustic solitary waves in magnetized dusty plasma with nonthermal electrons and trapped ions. The study examines the nonlinear propagation of dust-acoustic (DA) waves in magnetized dusty plasma, where small-amplitude solitary waves are described by the *K*d*V* equation. The plasma contains vortex-like trapped ions, nonthermal electrons, and negatively charged dust. They found that solitons are only rarefactive and DA waves cannot propagate below a critical nonthermal parameter β_c. Ion temperature ratios, magnetic field, dust gyrofrequency, and propagation obliqueness are some of the factors that affect soliton characteristics. Their results, which are backed by numerical analysis, demonstrate that solitons are resistant to turbulence and disturbances, which helps to clarify DA waves in lab and space plasmas, such as the Earth's magnetosphere and auroral regions. Maharaj *et al* [11] studied DAWs with negatively charged dust considering thermal electrons and nonthermal ions. They reported that the dust streaming and dust temperature could change the existence conditions that allowed negative and positive solitons to coexist. Abid *et al* [12] reported that DAWs show only rarefactive solitons when dust grains were taken negatively charged and electrons and ions follow nonthermal Cairns distribution. Recently, Zaidi *et al* [13] investigated three component DAWs in un-magnetized hot dust plasma with thermal ions and nonthermal electrons and found that the characteristics of solitons were substantially influenced by nonthermal parameters as well as the dust temperature.

Numerous investigations have demonstrated that the velocity distribution functions of constituent particles have a significant influence on the linear and nonlinear characteristics of plasma waves. The best choice for collisionless plasma in thermal equilibrium is the Maxwellian distribution. Observed space plasmas, on the other hand, typically exhibit nonthermal properties such as high energy particle abundance or a low energy flat top profile. A power law generalized Lorentzian or kappa distribution, developed by Vasyliunas [14], is used to model particles at the tail with high energy Masood *et al* [15]. Another nonthermal distribution function was presented by Cairns *et al* [16] to investigate the nonlinear character of plasma waves which were observed by Viking and Freja satellites. Cairns distribution then successfully interpreted the negative as well as positive polarity potential structures. However, the generalized (r, q) distribution function, established by Qureshi *et al* [17], not only helps us to study particles at high energy tails but flat tops or spiky distributed particles at low energies. This double spectral index distribution reduces to kappa distribution with limits $r = 0$, $q \to \kappa + 1$ and in Maxwellian distribution with limits $r = 0$, $q \to \infty$. In many problems, the (r, q) distribution was employed to explain such aspects of the waves that are unable to be described by the other nonthermal distributions [18–20]. In space plasmas, where plasma particles have low densities, non-Maxwellian distributions are the better choice to investigate nonlinear plasma waves and instabilities.

To the best of our knowledge, the co-existence of compressive and rarefactive solitons, when ions and electrons follow nonthermal distributions, has not been studied yet. Therefore, investigating the propagation characteristics of DAWs in the presence of Cairns distributed ions and (r, q) distributed electrons is the main objective of this research. It is also noted that because of the mathematical tractability, it is not possible to consider both the ions and electrons as (r, q) distributed.

2. Model equations

We examine un-magnetized dusty plasma consisting of three components: dust, ion and electron. The dust grains having negative charge are streaming in plasma where electrons and ions follow the Cairns distribution and (r, q) distribution, respectively. Charged neutrality at equilibrium is expressed as:

$$n_{i0} - n_{e0} - Z_d n_{d0} = 0. \tag{1}$$

In equation (1), n_{i0} defines the ion's number density at equilibrium, n_{e0} is the electron's number density at equilibrium and n_{d0} is the equilibrium number density of dust grains. Further, Z_d is a measure of an electron's density on a dust grain.

For the low phase-velocity DA waves, the dust dynamics are governed by the following set of equations:

$$\frac{\partial n_d}{\partial t} + \nabla\cdot(n_d \mathbf{v_d}) = 0, \tag{2}$$

$$\frac{\partial \boldsymbol{v_d}}{\partial t} + (\boldsymbol{v_d}\cdot\boldsymbol{\nabla})\boldsymbol{v_d} = \boldsymbol{\nabla}\varphi - \frac{\mu}{n_d}\boldsymbol{\nabla}P, \tag{3}$$

$$\frac{\partial P}{\partial t} + \boldsymbol{v_d}\cdot\boldsymbol{\nabla}P + \gamma P \quad \boldsymbol{\nabla}\cdot\boldsymbol{v_d} = 0. \tag{4}$$

The system is closed by Poisson's equation as follows:

$$\nabla^2\varphi = n_d + n_e - n_i. \tag{5}$$

In the above set of equations (2)–(5), $\mu(=T_d/Z_dT_i)$ describes the dust grains' normalized temperature and $\gamma[=(2+N)/N]$, where N is the degree of freedom. For 1D propagating wave we get $\gamma = 3$. Here n_d, n_i and n_e are dust, ion and electron densities, respectively, normalized by $Z_d n_{d0}$, φ is the electrostatic potential which is normalized by T_i/e, and dust pressure P is normalized by $n_{d0}k_BT_d$. Dust-acoustic speed $c_d = (Z_dk_BT_i/m_d)^{1/2}$ normalizes the dust velocity v_d; and $\lambda_d = (k_BT_i/4\pi Z_d n_{d0}e^2)^{1/2}$ and inverse of the dust frequency $\omega_{pd}^{-1} = (m_d/4\pi Z_d^2 n_{d0}e^2)^{1/2}$ are used to normalize space variable and time, respectively.

The electrons are nonthermal and assumed to follow the (r, q) distribution [17, 21–24] and the normalized number density for electrons can be written as [13],

$$n_e = n_{e0}(1 + \delta A_{rq}\varphi + \delta^2 B_{rq}\varphi^2), \tag{6}$$

where $\delta = T_i/T_e$ and A_{rq} and B_{rq} are the coefficients of the linear and nonlinear terms, respectively, which are given as

$$A_{rq} = \frac{(q-1)^{\frac{-1}{(1+r)}}}{2C}\frac{\Gamma\left(\frac{1}{2(1+r)}\right)\Gamma\left(q-\frac{1}{2(1+r)}\right)}{\Gamma\left(\frac{3}{2(1+r)}\right)\Gamma\left(q-\frac{3}{2(1+r)}\right)}, \tag{7}$$

$$B_{rq} = \frac{3(q-1)^{\frac{-2}{(1+r)}}}{8C^2}\frac{\Gamma\left(1-\frac{1}{2(1+r)}\right)\Gamma\left(q+\frac{1}{2(1+r)}\right)}{\Gamma\left(1+\frac{3}{2(1+r)}\right)\Gamma\left(q-\frac{3}{2(1+r)}\right)}, \tag{8}$$

where,

$$C = \frac{3(q-1)^{\frac{-1}{(1+r)}}\Gamma\left(q-\frac{3}{2(1+r)}\right)\Gamma\left(\frac{3}{2(1+r)}\right)}{2\Gamma\left(q-\frac{5}{2(1+r)}\right)\Gamma\left(\frac{5}{2(1+r)}\right)}. \tag{9}$$

The tail and flat top of the distribution's profile is measured by the spectral indices q and r, respectively; nonetheless these conditions must be fulfilled, $q > 1$ and $q(1+r) > 5/2$. The limiting case where kappa distribution is recovered from generalized (r, q) distribution function is $r = 0$ and $q = \kappa + 1$, and the constants A_{rq} and B_{rq} reduce to $A_\kappa = \frac{\kappa - 1/2}{\kappa - 3/2}$, $B_\kappa = \frac{(\kappa-1/2)(\kappa+1/2)}{2(\kappa-3)^2}$, respectively. Further, Maxwellian distribution can also be recovered from generalized (r, q) distribution under the limit $r = 0$ and $q \to \infty$, and the constants A_{rq} and B_{rq} reduce to $A_M = 1$, $B_M = 1/2$, respectively [25].

It is assumed that the ions are nonthermal as well and follow the Cairns distribution [16]. The normalized ion density is given by the following expression [7],

$$n_i = n_{i0}[1 + \beta\varphi + \beta\varphi^2]e^{-\varphi}, \tag{10}$$

where $\beta = \frac{4\alpha}{1+3\alpha}$.

Here, the nonthermal parameter α denotes the proportion of the nonthermal population. Maxwellian distribution can be retrieved in the limit $\alpha = 0$.

In order to obtain solutions for solitary waves, we convert our system into the stationary frame $\xi = x - Mt$, where M represents the velocity of solitary wave normalized by dust-acoustic-speed c_d. Re-writing the above set of equations (2)–(5), as

$$-M\frac{\partial n_d}{\partial \xi} + \frac{\partial (n_d v_d)}{\partial \xi} = 0, \tag{11}$$

$$-M\frac{\partial v_d}{\partial \xi} + v_d\frac{\partial v_d}{\partial \xi} = \frac{\partial \varphi}{\partial \xi} - \frac{\mu}{n_d}\frac{\partial P}{\partial \xi}, \tag{12}$$

$$-M\frac{\partial P}{\partial \xi} + v_d\frac{\partial P}{\partial \xi} + 3P\frac{\partial v_d}{\partial \xi} = 0, \tag{13}$$

$$\frac{\partial^2\varphi}{\partial \xi^2} = n_d + \rho(1 + \delta A_{rq}\varphi + \delta^2 B_{rq}\varphi^2) - \sigma(1 + \beta\varphi + \beta\varphi^2)e^{-\varphi}, \tag{14}$$

where, $\rho(=n_{e0}/Z_dn_{d0})$ and $\sigma(=n_{i0}/Z_dn_{d0})$. Integrate equations (11) and (13) applying the subsequent boundary constraints; $v_d \to v_{d0}$, $\varphi \to 0$, $n_d \to 1$ and $P \to 1$ at $|\xi| \to \pm\infty$, we get

$$n_d = \frac{(v_{d0} - M)}{(v - M)}, \tag{15}$$

$$P = n_d^3. \tag{16}$$

Here v_{d0} represents the dust drift velocity at equilibrium. Also, upon performing algebraic manipulations and supplanting equation (15) in equation (12), we derive the subsequent bi-quadratic equation

$$3\mu n_d^4 - \{(M - v_{d0})^2 + 3\mu + 2\varphi\}n_d^2 + (M - v_{d0})^2 = 0. \tag{17}$$

We solve equation (17), to get the solution for n_d as

$$n_d = \frac{\mu_1}{\sqrt{2}\ \mu_0}\times\sqrt{1 + \frac{2\varphi}{(M - v_{d0})\mu_1^2} - \sqrt{\left(1 + \frac{2\varphi}{(M - v_{d0})^2\mu_1^2}\right) - 4\frac{\mu_0^2}{\mu_1^4}}}, \tag{18}$$

where

$$\mu_0 = \sqrt{\frac{3\mu}{(M - v_{d0})^2}}, \text{ and } \mu_1 = \sqrt{1 + \mu_0^2}. \tag{19}$$

Setting dust streaming velocity $v_{d0} = 0$, in equations (17)–(18), expressions for n_d, μ_0 and μ_1 reduce to the expressions given in [7].

Using equation (18) in equation (14), yields

$$\frac{d^2\varphi}{d\xi^2} = \frac{\mu_1}{\sqrt{2}\ \mu_0}\left[1 + \frac{2\varphi}{(M - v_{d0})^2\mu_1^2} - \sqrt{\left(1 + \frac{2\varphi}{(M - v_{d0})^2\mu_1^2}\right)^2 - 4\frac{\mu_0^2}{\mu_1^4}}\right]^{\frac{1}{2}}$$

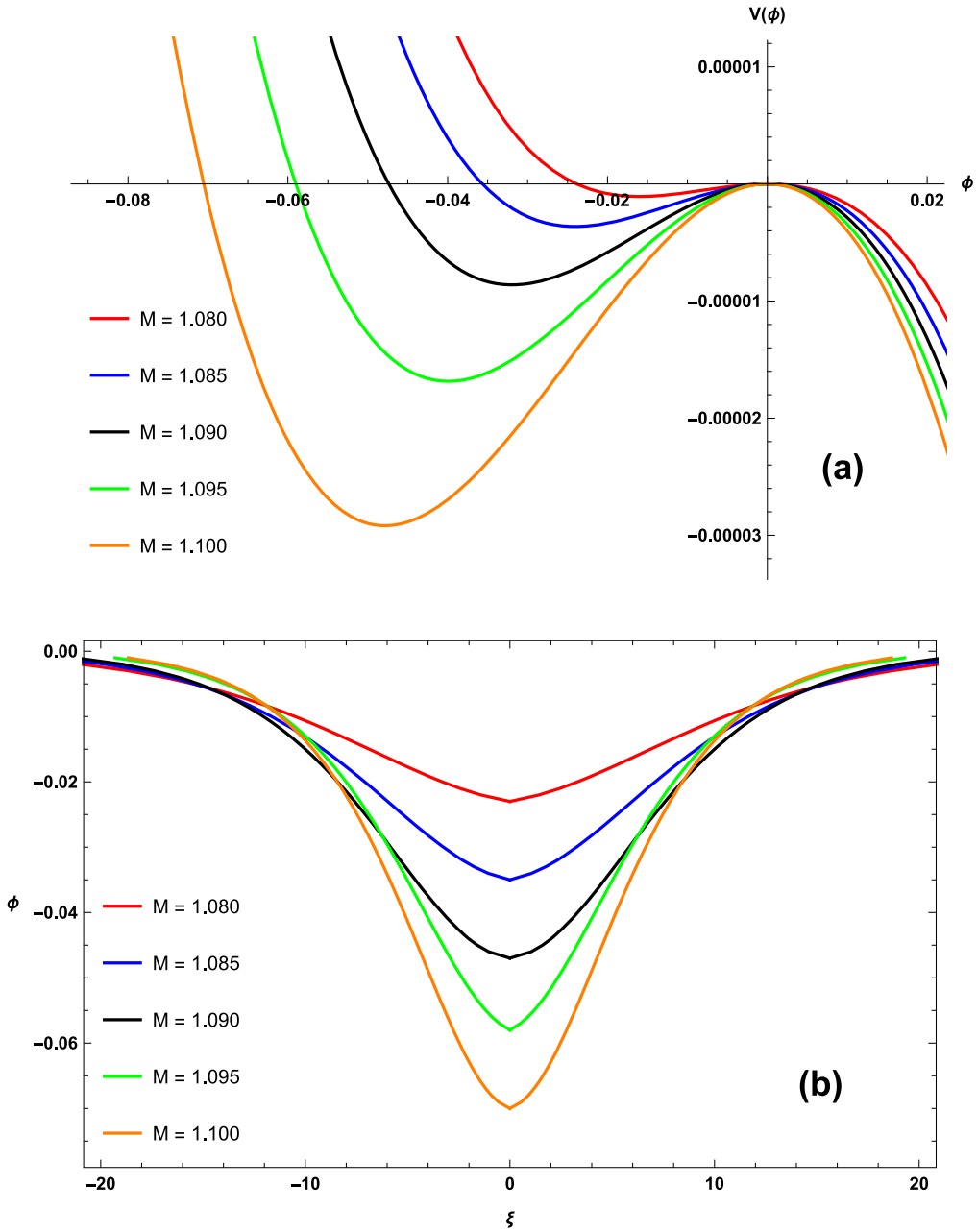

Figure 1. Sagdeev Potential (a) and corresponding soliton (b) for various values of Mach number M when $\alpha = 0$, $r = 2$, $q = 3$, $\mu = 0.02$, $\delta = 0.5$, $n_{e0} = 0.1$ $Z_d n_{d0}$ and $v_{d0} = 0.1\ c_d$.

$$+\rho(1 + \delta A_{rq}\varphi + \delta^2 B_{rq}\ \varphi^2) - \sigma(1 + \beta\ \varphi + \beta\varphi^2)\mathrm{e}^{-\varphi}. \tag{20}$$

Applying the Sagdeev potential technique [26] makes it easier to understand the qualitative nature of the solutions for equation (20). Therefore, after integration, it can be expressed as:

$$\frac{1}{2}\left(\frac{\mathrm{d}\varphi}{\mathrm{d}\xi}\right)^2 + V(\varphi) = 0, \tag{21}$$

where the Sagdeev potential, $V(\varphi)$, is given by

$$\begin{aligned} V(\varphi) = &-\sigma(1 + 3\beta(1 + \varphi) + \beta\varphi^2)\mathrm{e}^{-\varphi} \\ &-\rho\left(\varphi + \tfrac{1}{2}\delta A_{rq}\ \varphi^2 + \tfrac{1}{3}\delta^2 B_{rq}\ \varphi^3\right) \\ &-(M - v_{d0})^2\sqrt{\mu_0}\left(\exp\left[\frac{\epsilon}{2}\right] + \frac{1}{3}\exp\left[\frac{-3\epsilon}{2}\right]\right) + C_1. \end{aligned} \tag{22}$$

Here, C_1 is the constant of integration. Following Mendoza-Briceno *et al* [7], to enable the limit $\mu \to 0$ in the Sagdeev potential, for considering cold dust, we express ϵ as:

$$\epsilon = \ln\left[\frac{\mu_1^2}{2\mu_0^2}\left(1 + \frac{2\varphi}{(M - v_{d0})^2\mu_1^2}\right) + \sqrt{\frac{\mu_0^4}{4\mu_1^4}\left(1 + \frac{2\varphi}{(M - v_{d0})^2\mu_1^2}\right)^2 - 1}\right]. \tag{23}$$

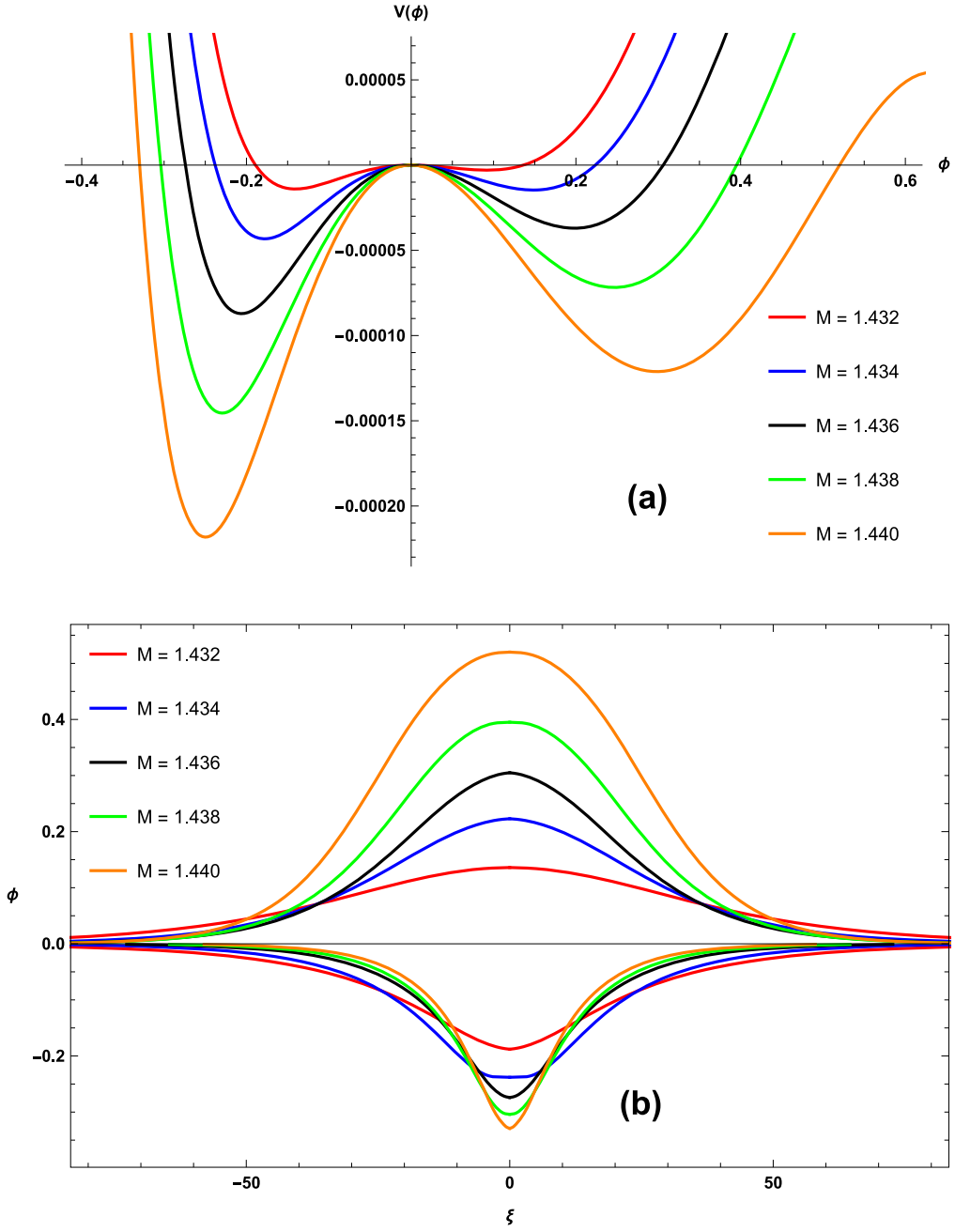

Figure 2. Sagdeev Potential (a) and corresponding soliton (b) for various values of Mach number M when $\alpha = 0.2$. The other parameters are the same as in figure 1.

By using above equation (23), the Sagdeev potential in equation (22) can be expressed as:

$$V(\varphi) = -\sigma(1 + 3\beta(1 + \varphi) + \beta\varphi^2)\mathrm{e}^{-\varphi} - \rho\left(\varphi + \frac{1}{2}\delta A_{rq}\,\varphi^2 + \frac{1}{3}\delta^2 B_{rq}\,\varphi^3\right) - \frac{(M - v_{d0})^2\mu_1}{\sqrt{2}}\sqrt{1 + \frac{2\varphi}{(M - v_{d0})^2\mu_1^2} + \sqrt{\left(1 + \frac{2\varphi}{(M - v_{d0})^2}\right)^2 - 4\frac{\mu_0^2}{\mu_1^4}}} - \frac{2\sqrt{2}\,\mu}{\mu_1^3}\left[1 + \frac{2\varphi}{(M - v_{d0})^2\mu_1^2} + \sqrt{\left(1 + \frac{2\varphi}{(M - v_{d0})^2}\right)^2 - 4\frac{\mu_0^2}{\mu_1^4}}\right]^{\frac{3}{2}} + C_1. \tag{24}$$

Similarly, at $\varphi = 0$, C_1 is computed for $V(\varphi) = 0$ and obtained, as

$$C_1 = \sigma(1 + 3\beta) + \frac{(M - v_{d0})^2\mu_1}{\sqrt{2}} \times \sqrt{1 + \sqrt{1 - 4\frac{\mu_0^2}{\mu_1^4}}} + \frac{2\sqrt{2}\,\mu}{\mu_1^3}\left[1 + \sqrt{1 - 4\frac{\mu_0^2}{\mu_1^4}}\right]^{-\frac{3}{2}}. \tag{25}$$

Equation (24) describes the Sagdeev potential. The conditions given below must be met in order to derive solitary solutions from equation (24) [23].

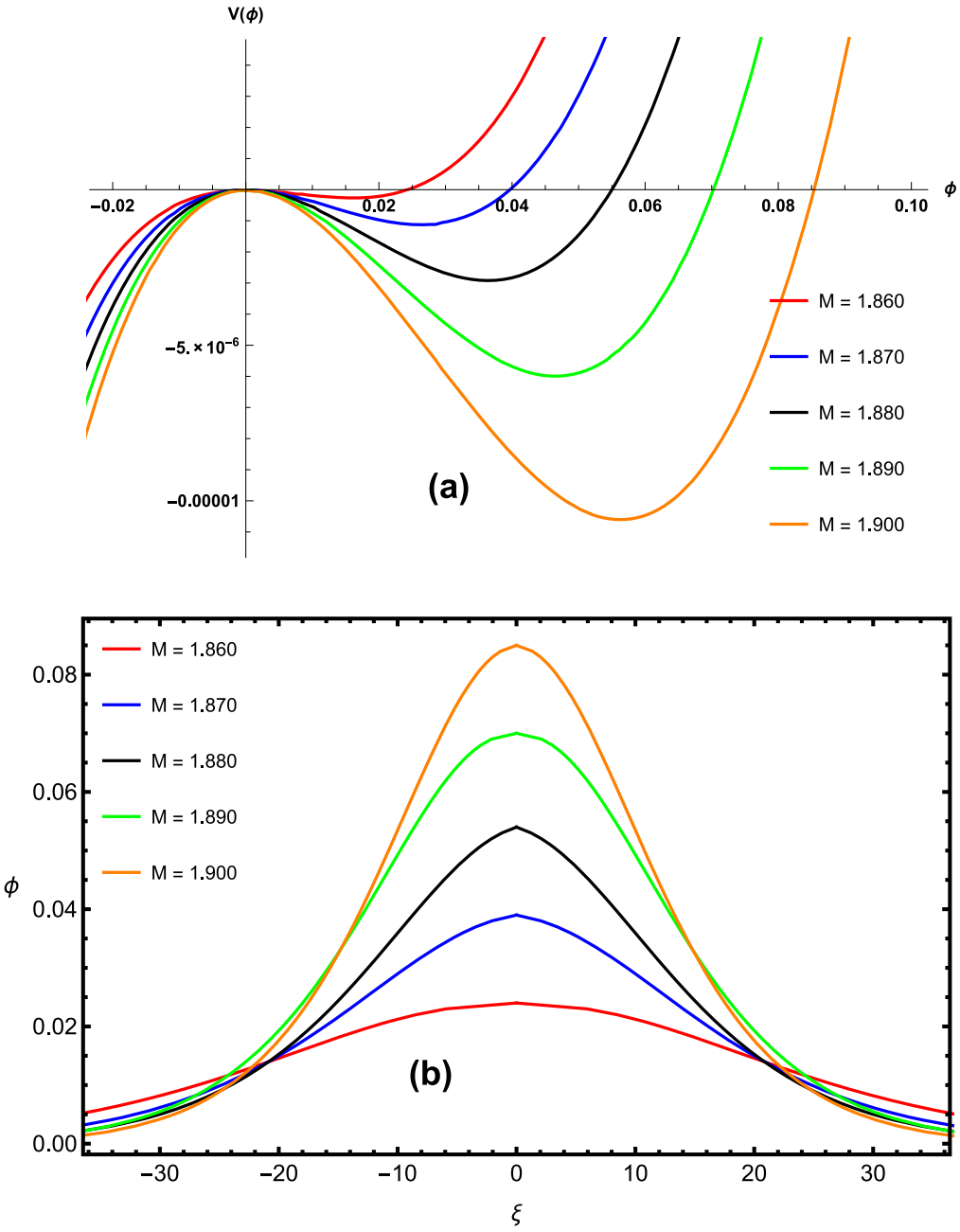

Figure 3. Sagdeev Potential (a) and corresponding soliton (b) for various values of Mach number M when $\alpha = 0.4$. The other parameters are the same as in figure 1.

$$V(\varphi)|_{\varphi=0} = 0\,,\ V'(\varphi)|_{\varphi=0} = 0\,,\ V''(\varphi)|_{\varphi=0} < 0,$$

$$V(\varphi)\,|_{\varphi=\varphi_{\max}} = 0\,,\ V'(\varphi)\,|_{\varphi=\varphi_{\max}} > 0$$

for compressive solitary structures,

$$V(\varphi)\,|_{\varphi=\varphi_{\min}} = 0\,,\ V'(\varphi)\,|_{\varphi=\varphi_{\min}} < 0$$

for rarefactive solitary structures.

Following the Taylor expansion of the Sagdeev potential $V(\varphi)$ in equation (24) about the origin, the critical Mach number (M_c), at which the second derivative's sign changes, is defined as

$$M_c = \sqrt{\frac{1 + 3\mu(\sigma(1-\beta) + \delta A_{rq}\rho)}{\sigma(1-\beta) + \delta A_{rq}\rho}} + v_{d0}. \tag{26}$$

Equation (26) shows the threshold for the existence of solitary structure. In the case where $M > M_c$, the Sagdeev potential in equation (24) would result in solitary structure (compressive or rarefactive or both). For a limiting scenario when electrons are thermally (Maxwellian) distributed i.e. $A_{rq} \to 1$, equation (26) reduces to equation (31) of Maharaj *et al* [11]. However, when ions follow Maxwellian (thermal) distribution i.e. $\alpha \to 0$, equation (26) agrees with equation (26) of Zaidi *et al* [13]. Furthermore, in the absence of dust streaming and electron number density i.e. $v_{d0} = n_{e0} = 0$,

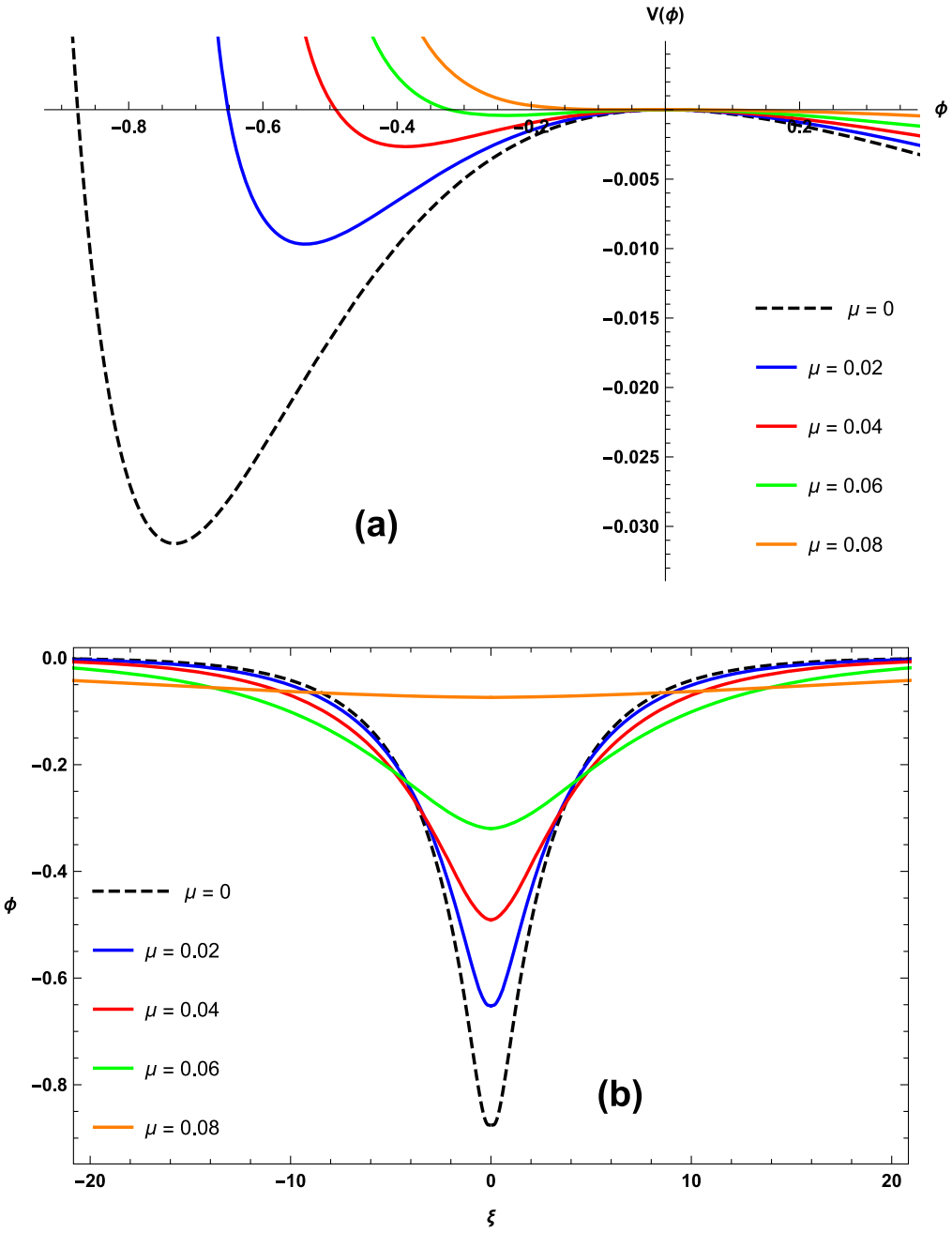

Figure 4. Sagdeev Potential (a) and corresponding soliton (b) for various values $\alpha = 0.2$ and $M = 1.50$ when $\alpha = 0.2$ and $M = 1.50$. The other parameters are the same as in figure 1.

equation (26) agrees with equation (30) of Mendoza-Briceno *et al* [7].

3. Numerical results

The dust acoustic solitary structures (DASS) are investigated in this section to study the dependence of solitary structures on different nonthermal parameters based on the choice of the distribution function. Since the plasma particles usually are not in thermal equilibrium and are streaming in laboratory or space environments, we can better understand the actual physical situations in such circumstances by employing nonthermal distributions in theoretical models. Therefore, we have taken into account the influence of dust streaming in this study while exploring Cairns distributed ions and (r, q) distributed electrons in an un-magnetized dusty plasma. For numerical purposes, we use observed plasma parameters from planetary rings of Saturn [27, 28]. The chosen parameters are based on the Cassini spacecraft's local measurements near the primary A and B rings and are: $n_{e0} = (2-45) \times 10^6\,\mathrm{m}^{-3}$, $n_{i0} = (1 - 20) \times 10^6\,\mathrm{m}^{-3}$, $n_{d0} = (10^3 - 10^5)\ \ \mathrm{m}^{-3}$, $\ m_d = 4 \times 10^{-15}\mathrm{kg}$, $\ Z_d = 100$, $T_i < T_e = 1-10$ eV, $T_d = 0.01$ eV.

The Sagdeev potential and associated soliton for Maxwellian ions (i.e. $\alpha = 0$) are plotted in figure 1, however, electrons follow (r, q) distribution ($r = 2$, $q = 3$). For a range

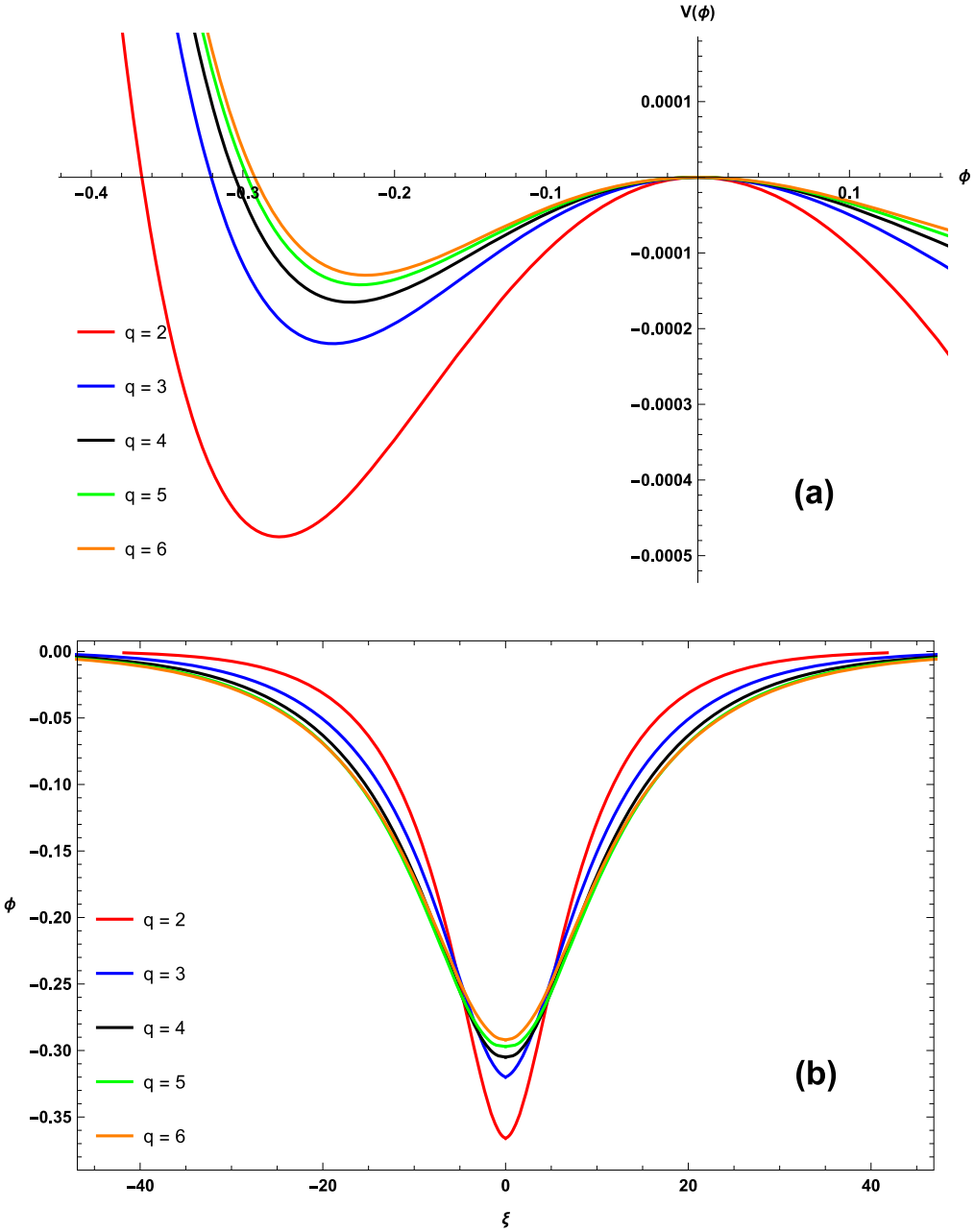

Figure 5. Sagdeev Potential (a) and corresponding soliton (b) for various values of q when $r = 1$, $\alpha = 0.2$ and $M = 1.435$. The other parameters are the same as in figure 1.

of M values, the Sagdeev potential with negative polarity is shown in figure 1(a) while figure 1(b) shows the associated solitons. It can be seen that only negative potential solitary structures exist when ions are Maxwellian and electrons are nonthermal, i.e. (r, q) distributed; which agrees with the past investigations that thermal ion distribution supports only rarefactive structures [5, 11–13]. Furthermore, as M increases, the soliton amplitude increases.

In figure 2, the Sagdeev potential and associated solitons are plotted for different M when both ions and electrons are nonthermal. We can see that as the nonthermal parameter for ions reaches a certain value, i.e. $\alpha = 0.2$ with the same values of r and q as in figure 1, both compressive and rarefactive Sagdeev potential structures co-exist (figure 2(a)). Likewise, associated solitons, both compressive and rarefactive, are shown in figure 2(b). It can be seen that as M increases, soliton's amplitude increases while its width decreases, for the rarefactive as well as compressive structures. However, for $\alpha = 0.1$ and $r = 2$, $q = 3$, we get rarefactive structures only, not shown here. Earlier, Abid *et al* [12] showed that only rarefactive structures could exist when ions and electrons both follow a nonthermal distribution. However, our study reveals that compressive and rarefactive structures can coexist.

In figure 3, the Sagdeev potential and associated solitons are plotted for different M when $\alpha = 0.4$ and $r = 2$, $q = 3$. We can note that as the nonthermal parameter for ions further increases, i.e. $\alpha \geqslant 0.26$, we can only obtain the positive

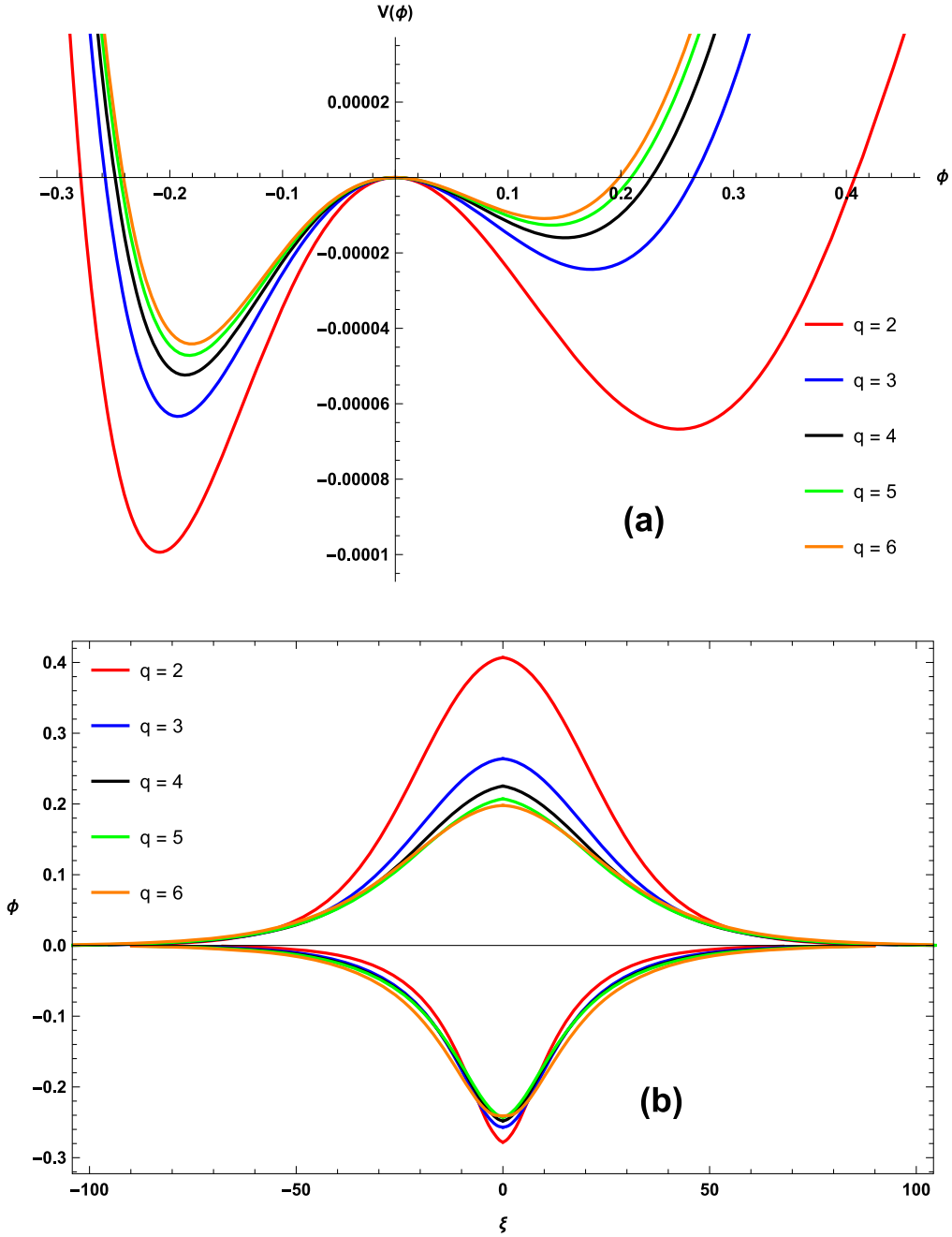

Figure 6. Sagdeev Potential (a) and corresponding soliton (b) for various values of q when $r = 2$. The other parameters are same as in figure 5.

polarity Sagdeev potential structures (figure 3(a)). Figure 3(b) portrays the soliton corresponding to the Sagdeev potential in figure 3(a). It is evident that when M increases, the soliton amplitude likewise increases but its width decreases. Hence, from figures 2 and 3, it is observed that there is a transition in the DASS, from negative to positive with the co-existence in between, that depends on the nonthermal parameter α for ions when electrons follow flat-topped (r, q) distribution.

In figure 4, the Sagdeev potential and associated soliton are plotted for different values of dust to ion temperature ratio $\mu(=T_d/Z_d T_i)$ when $\alpha = 0.2$, $q = 3$, $r = 2$ and $M = 1.5$. The Sagdeev potential with negative polarity for different values of μ is shown in figure 4(a), while the associated solitons are shown in figure 4(b). It is evident that as μ increases the amplitude decreases which also agrees with the earlier findings [7, 12, 13].

In figure 5, the Sagdeev potential and associated solitons are plotted for different values of q when $\alpha = 0.2$, $r = 1$ and $M = 1.435$. Figure 5(a) shows the rarefactive Sagdeev potentials for different q's and associated solitons in figure 5(b). It is evident that when q decreases, the rarefactive soliton amplitude increases, which means the electrons in high energy tails are responsible for the increase in soliton's amplitude. In figure 6, the Sagdeev potential and associated soliton are plotted for different values q for $\alpha = 0.2$ but $r = 2$. We can see that as the value of r increases from

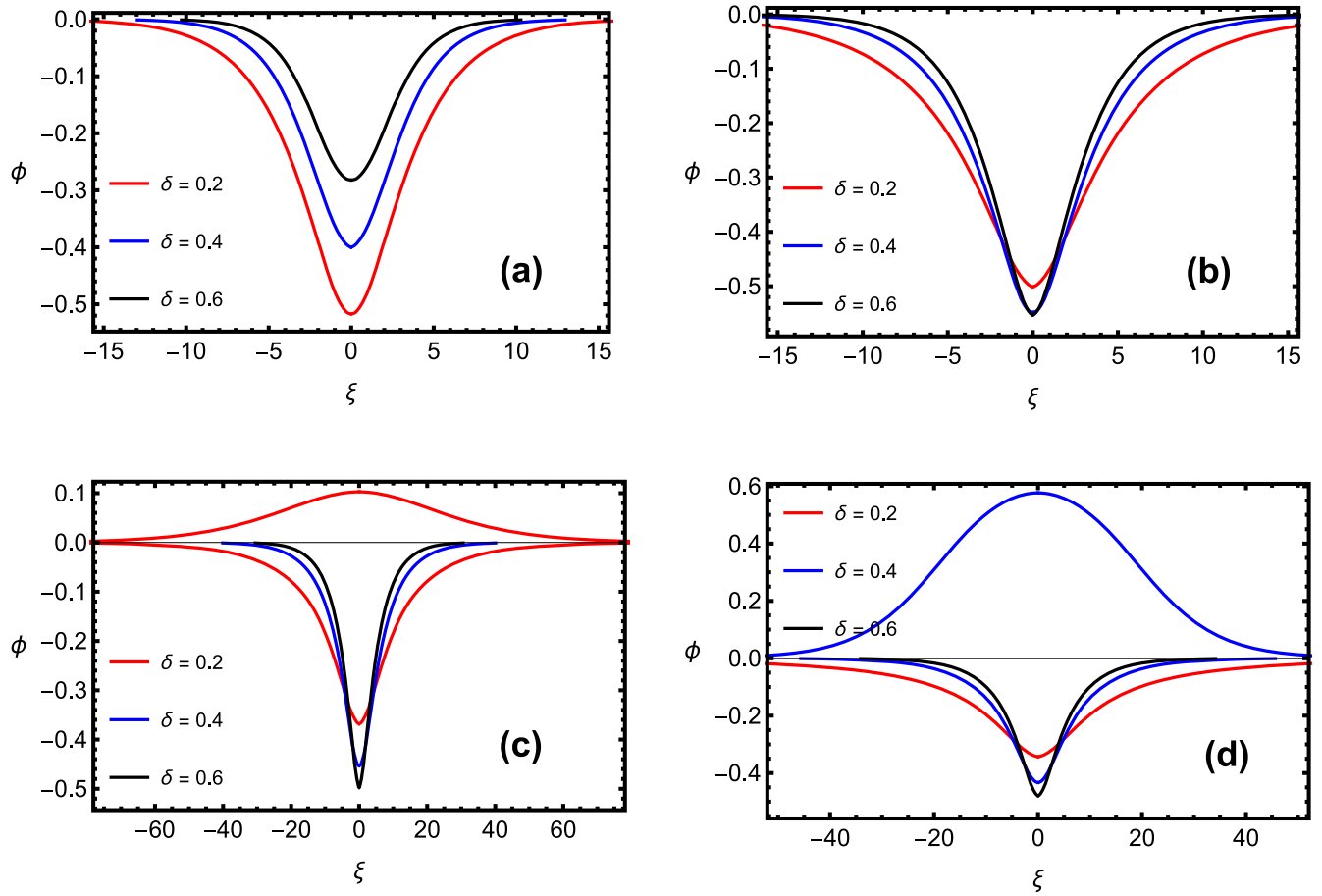

Figure 7. Solitons for various values of $\delta(=T_i/T_e)$ for (a) $r=-0.1$, (b) $r=0$, (c) $r=1$ and (d) $r=2$, when $q=3$, $M=1.455$ and $\alpha=0.2$. The other parameters are same as figure 1.

$r=1$ to $r=2$ (as compared to figure 5), the flat-topped profile of electrons is enhanced, and we obtain simultaneous existence of both polarities of Sagdeev potentials and corresponding solitons. For rarefactive and compressive structures, it is evident that as q decreases, the width of soliton also decreases but amplitude increases.

In figure 7, we plot the solitons for various values of ion to electron temperature ratios $\delta(=T_i/T_e)$ when $q=3$, $\alpha=0.2$ and $M=1.455$. Figure 7(a) shows the solitons for various values of δ when $r=-0.1$. For the spiky electron distribution ($r=-0.1$), it is seen that when the temperature ratio δ decreases, the width and amplitude of rarefactive solitons increase, i.e. for colder ions the amplitude is higher. Figure 7(b) shows the solitons for different values of δ when $r=0$. For the electron exhibiting kappa distribution (i.e. $r=0$, $q=3$), soliton amplitude increases but width decreases with the increase in δ. Figure 7(c) shows the solitons for different values of δ when $r=1$. For flat-topped electron distribution, the co-existence of rarefactive and compressive soliton is observed for $\delta=0.2$, however, with further increase in δ only rarefactive solitons are obtained whose amplitude increases but width decreases with the increase in δ. Figure 7(d) shows the solitons for different values of δ but for $r=2$. Here, it is observed that solitons with different polarity coexist for the larger value of temperature ratio, i.e. $\delta=0.4$. Though width decreases but amplitude increases with the increase in δ, for solitons with positive as well as negative polarities.

In figure 8, the Sagdeev potential and associated soliton are plotted for different values of positive r when $q=3$ and $\alpha=0.2$. It can be seen that for $r\geqslant 2$, rarefactive and compressive solitons coexist whose amplitude decreases as r increase, i.e. the enhanced flat-top electron distribution profile is responsible for the formation of dual polarity. In figure 9, the Sagdeev potential and associated soliton are plotted for different values of negative r when $q=5$ and $\alpha=0.2$. For spiky distribution (i.e. $r<0$), only rarefactive solitons are observed and as the negative value of r decreases the amplitude increases. Additionally, it is evident that the soliton's amplitude stays lower than the Maxwellian for $r<-0.2$.

In figure 10, we plot Sagdeev potentials for various combinations of distributions. We can see that when both ions and electrons follow Maxwellian distribution, i.e. $\alpha=0$ and $r=0$, $q\to\infty$, respectively, only negative potential structures are obtained, which coincides with the results of Rao *et al* [1]. In the second case, when ions behave thermally and follow Maxwellian distribution ($\alpha=0$), but electrons follow flat-topped distribution ($r=2$, $q=3$), again only negative

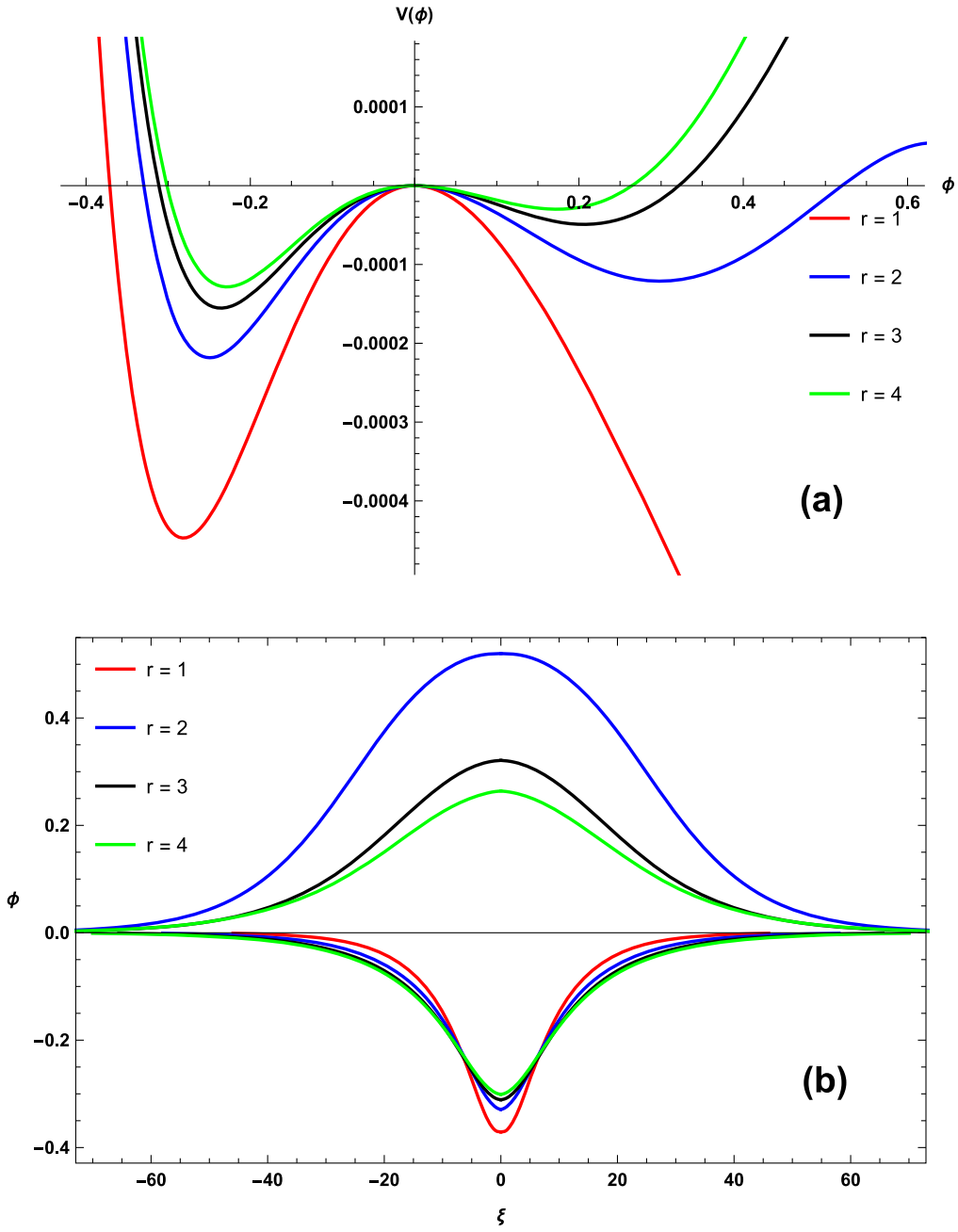

Figure 8. Sagdeev Potential (a) and corresponding soliton (b) for various values of r when $q = 3$, $M = 1.44$ and $\alpha = 0.2$. The other parameters are the same as figure 1.

potential structures are obtained, which agrees with the results of Zaidi *et al* [13]. Moreover, when ions follow Cairns distribution ($\alpha = 0.22$), but electrons follow Maxwellian distribution ($r = 0$, $q \to \infty$), both positive and negative polarity Sagdeev potential structures are obtained the same as that obtained by Maharaj *et al* [11]. For the case of the current study, when ions follow Cairns distribution ($\alpha = 0.20$) and electrons follow flat-topped distribution ($r = 2$, $q = 3$), we found that both positive and negative polarity solitary structures coexist. However, in a recent study, Abid *et al* [12] found only rarefactive solitons when ions and electrons followed Cairns distribution.

4. Summary and conclusion

To account for the impact of low energy and high energy particles in the profile of distribution functions, we have studied the DA soliton's amplitude and width characteristics in un-magnetized dusty plasma. In this work, the pseudopotential method for obtaining the solutions for solitary waves using fluid equations has been taken into consideration. It was previously established that when both electrons and ions followed nonthermal distributions, only rarefactive solitary solutions were feasible [12]. However, in the current study, we not only found compressive and rarefactive structures

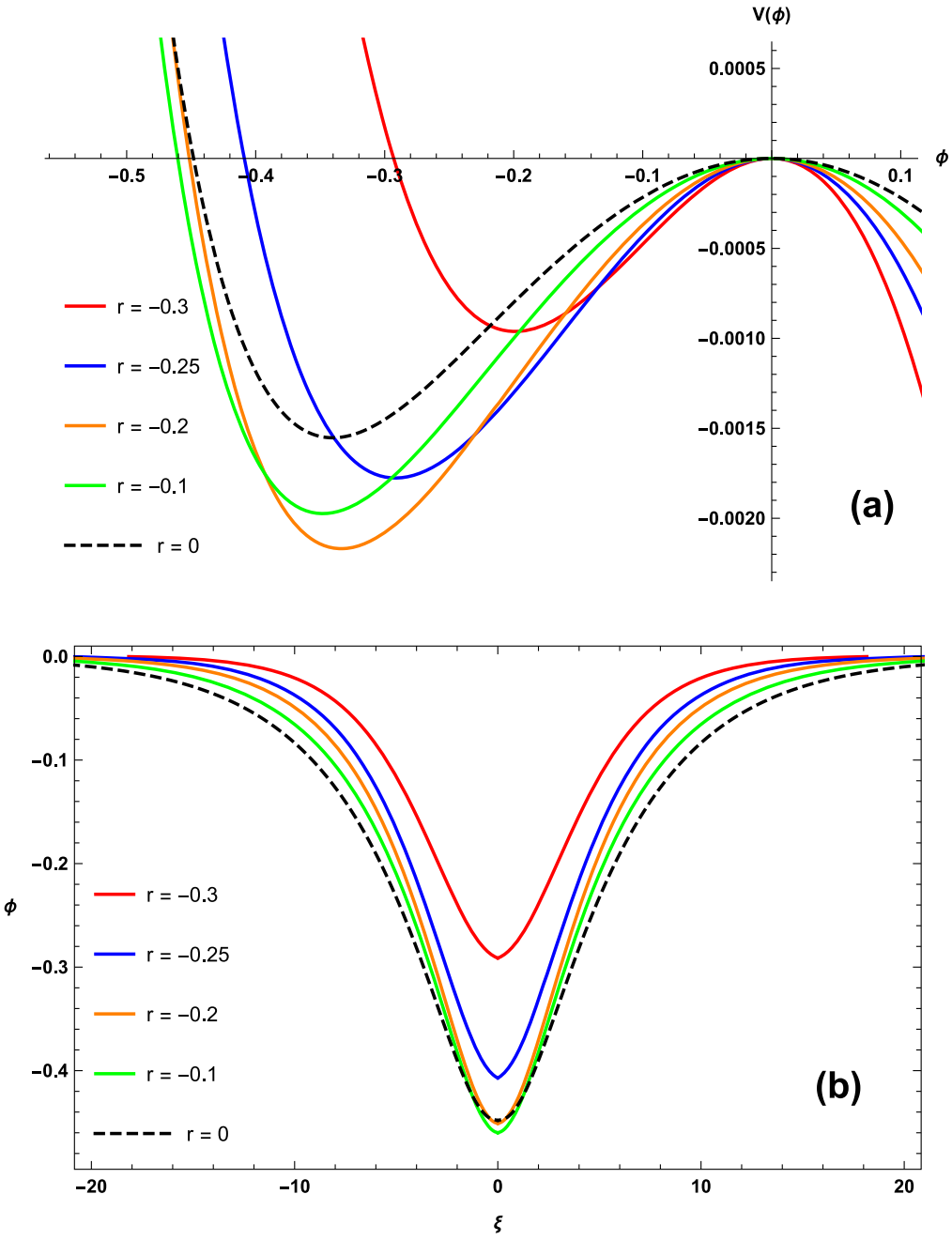

Figure 9. Sagdeev Potential (a) and corresponding soliton (b) for various values of negative r when $q = 5$. The other parameters are same as figure 8.

independently but their co-existence also when ions and electrons follow Cairns and (r, q) distributions, respectively. Our findings demonstrated that the nonthermal spectral indices r, q and α have a significant influence on the soliton's width and amplitude. Our results also showed a significant transition in the polarity of soliton, rarefactive to compressive structure with the co-existence in between, as the nonthermal parameter α increases. With an increase in dust to ion temperature ratio we have observed a decrease in the amplitude of soliton. We also found that for the spiky electron distribution ($r < 0$), the amplitude of negative polarity solitons increases with decreasing δ, but decreases with the increase in negative values of r. For the kappa electron distribution ($r = 0$, $q > 2$), soliton amplitude increases but width decreases. However, for flat top electron distribution ($r > 0$), the co-existence of rarefactive and compressive soliton is observed and the amplitude of soliton increases with increasing δ, but decreases with increasing r. Moreover, the soliton's amplitude is higher for smaller values of q, i.e. the increase in the amplitude with the increase in high energy particles. Finally, it is concluded that the characteristics of DASS are conspicuously altered by the electron and ion distribution profiles. In the case of nonthermal ions, irrespective of electrons, the co-existence of positive and negative solitary structures is possible. However, if electrons and ions follow the same distribution function, only rarefactive

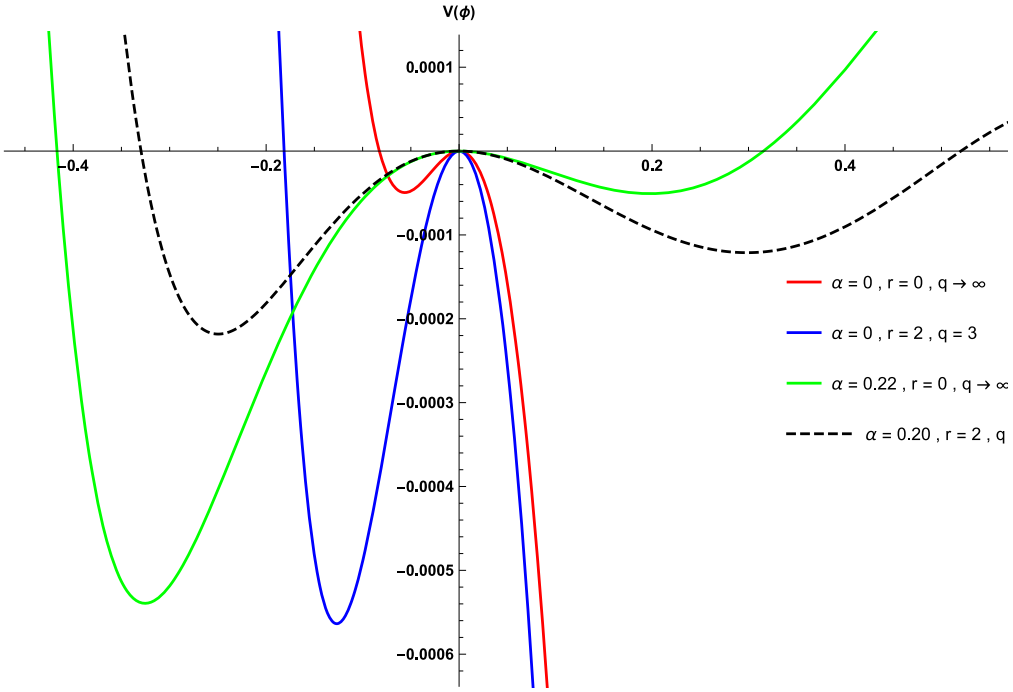

Figure 10. Sagdeev Potential for various values of α, r and q. The other parameters are same as figure 1.

structures can be obtained. Thus the results presented in the current study are helpful in interpreting the propagation characteristics of DASS based on the low and high energy particles in the profile of nonthermal distribution functions in various space environments.

Author contributions

All authors have equal contributions in Conceptualization, methodology, formal analysis, investigation, writing—original draft preparation.

ORCID iDs

S A M Zaidi https://orcid.org/0009-0001-2668-6771
M N S Qureshi https://orcid.org/0000-0003-3909-6305
Saba Khalid https://orcid.org/0000-0001-8942-8051

References

[1] Rao N N, Shukla P K and Yu M Y 1990 Dust-acoustic waves in dusty plasmas *Planet. Space Sci.* **38** 543–6
[2] Barkan A, Merlino R L and D'Angelo N 1995 Laboratory observation of the dust-acoustic wave mode *Phys. Plasmas* **2** 3563–5
[3] Praburam G and Goree J 1996 Experimental observation of very low-frequency macroscopic modes in a dusty plasma *Phys. Plasmas* **3** 1212–9
[4] Abd-Elzaher M and Atteya A 2022 Negative energy dust acoustic waves evolution in a dense magnetized quantum Thomas–Fermi plasma *Sci. Rep.* **12** 15890
[5] Mamun A A, Cairns R A and Shukla P K 1996 Solitary potentials in dusty plasmas *Phys. Plasmas* **3** 702–4
[6] Asgari H, Muniandy S V and Wong C S 2013 Dust-acoustic waves in dusty plasmas with non-thermal ions *Phys. Plasma* **20** 23705
[7] Mendoza-Briceno C A, Russel S M and Mamun A A 2000 Large amplitude electrostatic solitary structures in a hot non-thermal dusty plasma *Planet. Space Sci.* **48** 599–608
[8] Gill T S and Kaur H 2000 Effect of nonthermal ion distribution and dust temperature on nonlinear dust acoustic solitary waves *Pramana* **55** 855–9
[9] Mahmood S and Saleem H 2003 Dust acoustic solitary wave in the presence of dust streaming *Phys. Plasmas* **10** 47–52
[10] Misra A P and Wang Y 2015 Dust-acoustic solitary waves in a magnetized dusty plasma with nonthermal electrons and trapped ions *Commun. Nonlinear Sci. Numer. Simulat.* **22** 1360–9
[11] Maharaj S K, Pillay S R, Bharuthram R, Singh S V and Lakhina G S 2004 The effect of dust grain temperature and dust streaming on electrostatic solitary structures in a non-thermal plasma *Phys. Scr.* **T113** 135–40
[12] Abid A A, Zhengwei W, Khan A, Qureshi M N S and Esmaeili A 2023 Formation of dust acoustic rarefactive solitary structures in a Cairns distributed electron–ion plasma *AIP Adv.* **13** 105012
[13] Zaidi S A M, Qureshi M N S and Khalid S 2024 Effect of nonthermal electron distributions on dust acoustic solitons in cometary plasmas *AIP Adv.* **14** 025122
[14] Vasyliunas V M 1968 A survey of low-energy electrons in the evening sector of the magnetosphere with OGO 1 and OGO 3 *J. Geophys. Res.* **73** 2839–84
[15] Masood W, Qureshi M N S, Yoon P H and Shah H A 2015 Nonlinear kinetic Alfvén waves with non-Maxwellian electron population in space plasmas *J. Geophys. Res. Space Phys.* **120** 101–12

[16] Cairns R A, Mamum A A, Bingham R, Bostrom R, Dendy R O, Nairn C M C and Shukla P K 1995 Electrostatic solitary structures in non-thermal plasmas *Geophys. Res. Lett.* **22** 2709
[17] Qureshi M N S, Shah H A, Murtaza G, Schwartz S J and Mahmood F 2004 Parallel propagating electromagnetic modes with the generalized (r, q) distribution function *Phys. Plasmas* **11** 3819–29
[18] Shumaila J, Saba R F, Alrowaily A W and El-Tantawy S A 2024 On the oblique electrostatic waves in a dusty plasma with non-Maxwellian electrons for Saturn's magnetosphere *J. Low Freq. Noise Vib. Act. Control.* **43** 170–81
[19] Nasir W, Ehsan Z, Qureshi M N S and Shah H A 2019 Solar wind driven electrostatic instabilities with generalized (r, q) distribution function *Contrib. Plasma Phys.* **59** e201800159
[20] Kouser S, Shah K H, Qureshi M N S and Shah H A 2020 Nonlinear ion-acoustic waves in *e–p–i* plasmas with (r, q) distributed electrons and positrons *AIP Adv.* **10** 055123
[21] Shah K H, Qureshi M N S, Masood W and Shah H A 2018 Electron acoustic nonlinear structures in planetary magnetospheres *Phys. Plasmas* **25** 042303
[22] Khalid S, Qureshi M N S and Masood W 2019 Compressive and rarefactive solitary structures of coupled kinetic Alfven-acoustic waves in non-Maxwellian space plasmas *Phys. Plasmas* **26** 092114
[23] Khalid S, Qureshi M N S and Masood W 2020 Alfvenic perturbations with finite Larmor radius effect in non-Maxwellian electron–positron–ion plasmas *AIP Adv.* **10** 25002
[24] Raffah B M, Abid A A, Khan A, Esmaeili A, Al-Hadeethi and Qureshi M N S 2004 Dust particle surface potential in an argon-helium plasma using the (r, q)-distribution function *Commun. Theo. Phys.* **76** 095501
[25] Qureshi M N S, Shah K H, Shi J K, Masood W and Shah H A 2019 Investigation of cubic nonlinearity-driven electrostatic structures in the presence of double spectral index distribution function *Contrib. Plasma Phys.* **60** e201900065
[26] Sagdeev R Z 1966 Cooperative phenomena and shock waves in collisionless plasmas *Rev. Plasma Phys.* **4** 23 (https://api.semanticscholar.org/CorpusID:62787591)
[27] Yaroshenko V V, Verheest F and Morfill G E 2007 Dust-acoustic waves in collisional dusty plasmas of planetary rings *Astron. Astro.* **461** 385–91
[28] Bezbaruah T and Karmakar P K 2024 Nonlinear dust-acoustic wave dynamics in nonthermal Saturnian E-ring with negative ion moderation *Chin. J. Phys.* **89** 1611–23